

1    **Supplementary Information**

2    **Multiple pathways for the formation of secondary organic aerosol in North China Plain**  
 3    **in summer**

4    Yifang Gu<sup>1,4</sup>, Ru-Jin Huang<sup>1,2,3,4</sup>, Jing Duan<sup>1</sup>, Wei Xu<sup>1</sup>, Chunshui Lin<sup>1</sup>, Haobin Zhong<sup>1,4</sup>, Ying  
 5    Wang<sup>1</sup>, Haiyan Ni<sup>1</sup>, Quan Liu<sup>5</sup>, Ruiguang Xu<sup>6,7</sup>, Litao Wang<sup>6,7</sup>, Yong Jie Li<sup>8</sup>

6

7

8    **Table S1.** Summary of Mass Concentrations of PM<sub>2.5</sub> Species and OA Components ( $\mu\text{g m}^{-3}$ ), Mixing  
 9    Ratios of gas-phase pollutants, and meteorological parameters in the Summer Studies in Handan.

	Handan Summer			
	All	P1	P2	P3
Total	37.3 $\pm$ 19.0	29.3 $\pm$ 12.7	36.0 $\pm$ 14.7	64.1 $\pm$ 29.4
OA	19.6 $\pm$ 5.5	15.4 $\pm$ 3.2	19.8 $\pm$ 4.7	25.0 $\pm$ 6.2
HOA	2.4 $\pm$ 2.1	2.2 $\pm$ 1.5	2.6 $\pm$ 2.5	1.7 $\pm$ 1.1
COA	3.7 $\pm$ 2.6	4.6 $\pm$ 3.3	3.1 $\pm$ 2.2	3.4 $\pm$ 2.8
primary-SOA	1.0 $\pm$ 1.2	1.0 $\pm$ 1.3	1.0 $\pm$ 1.2	0.7 $\pm$ 1.4
fresh-SOA	3.5 $\pm$ 2.5	3.5 $\pm$ 1.3	4.0 $\pm$ 2.3	5.5 $\pm$ 2.7
phochem-SOA	6.1 $\pm$ 3.3	6.1 $\pm$ 1.9	7.3 $\pm$ 3.1	5.4 $\pm$ 2.4
aq-SOA	3.9 $\pm$ 3.5	2.9 $\pm$ 2.2	1.8 $\pm$ 2.0	8.3 $\pm$ 6.3
Sulfate	7.2 $\pm$ 4.9	5.9 $\pm$ 5.8	7.1 $\pm$ 4.0	11.8 $\pm$ 6.2
Nitrate	4.3 $\pm$ 6.3	3.5 $\pm$ 2.9	3.0 $\pm$ 4.4	14.9 $\pm$ 11.3
Ammonium	2.7 $\pm$ 2.5	2.2 $\pm$ 1.9	2.4 $\pm$ 1.7	6.5 $\pm$ 4.1
Chloride	0.4 $\pm$ 0.6	0.3 $\pm$ 0.3	0.4 $\pm$ 0.6	1.0 $\pm$ 1.1
BC	3.1 $\pm$ 2.0	2.0 $\pm$ 1.2	3.3 $\pm$ 1.9	4.9 $\pm$ 2.4
CO(ppm)	0.8 $\pm$ 0.7	0.6 $\pm$ 0.6	0.8 $\pm$ 0.8	1.3 $\pm$ 0.5
NO <sub>2</sub> (ppb)	14.4 $\pm$ 9.9	11.8 $\pm$ 5.3	15.6 $\pm$ 11.7	15.9 $\pm$ 5.4
SO <sub>2</sub> (ppb)	4.0 $\pm$ 4.6	2.4 $\pm$ 2.5	5.2 $\pm$ 5.5	2.2 $\pm$ 1.5
O <sub>3</sub> (ppb)	54.0 $\pm$ 22.8	24.0 $\pm$ 14.5	49.5 $\pm$ 29.1	32.2 $\pm$ 24.6
WS(m/s)	1.5 $\pm$ 1.0	1.7 $\pm$ 1.1	1.6 $\pm$ 1.0	1.0 $\pm$ 0.6
WD(°)	187.1 $\pm$ 121.8	223.1 $\pm$ 126.6	168.2 $\pm$ 111.5	201.9 $\pm$ 124.4
T(°C)	25.0 $\pm$ 4.3	22.3 $\pm$ 2.8	26.4 $\pm$ 4.0	23.1 $\pm$ 2.6
RH(%)	66.3 $\pm$ 19.4	79.4 $\pm$ 13.0	57.7 $\pm$ 17.5	83.7 $\pm$ 12.5
ALWC	21.4 $\pm$ 51.3	22.6 $\pm$ 48.0	8.4 $\pm$ 15.8	95.4 $\pm$ 114.2

10

11

12

13

14

15

16

17

18

19

20

21

22

23

24 **Table S2.** Concentrations of the main chemical components in PM<sub>1</sub>/PM<sub>2.5</sub> during summer and winter  
25 observations in NCP in recent years.

26

Sites	OA	SO <sub>4</sub>	NO <sub>3</sub>	NH <sub>4</sub>	Cl	BC	PM	PM <sub>1</sub>	NR-PM <sub>1</sub>	PM <sub>2.5</sub>
Our study	19.0	7.2	4.3	2.7	0.4	3.1				36.7
2013 Summer, Handan (Zhao et al., 2019)		16.1	16.5	7.3	3.3					95.6
2017 Summer, Handan (Zhao et al., 2019)		13.4	5.0	6.2	0.7					64.8
2015 winter, Handan (Li et al., 2017)	81.2	28.1	26.1	21.4	16.6	9.4		187.6	173.4	
2018 Summer, Beijing (Xu et al., 2019b)	12.7	6.5	7.4	4.3	0.2					31.1
2018 Summer, Beijing (Chen et al., 2020)	12.2	3.9	2.5	2.2	0.1	3.2		24.1		
2019 Summer, Beijing (Chen et al., 2020)	9.3	4.5	2.8	2.5	0.2			19.3		
2019 Summer, Xian (Duan et al., 2020)	14.0	3.9	2.8	1.7	0.1					22.5

27

28

29

30

31

32

33

34

35

36

37

38

39

40

41

42

43

44

45 **Table S3.** Elemental ratios and OM:OC ratios in OA obtained from field observations at urban and  
 46 rural/suburban sites. The ratios are corrected by the “improved-ambient” method (Canagaratna et al.,  
 47 2015).

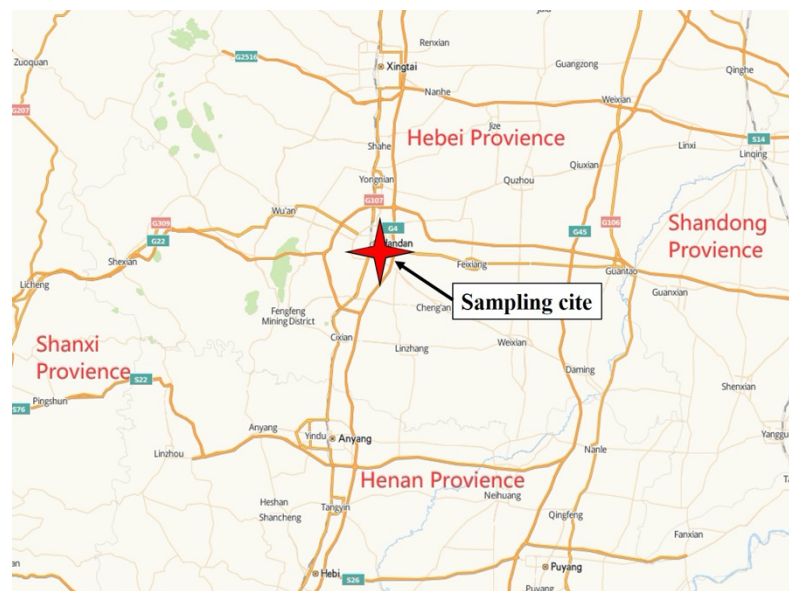
48

sites	site types	seasons	H:C	O:C	OM:OC	ref
our study	urban	summer 2019	1.58	0.75	2.17	
	suburban	summer 2018	1.67	0.54	1.89	Chen et al.2020b
		summer 2012	1.63	0.53	1.88	
Beijing	urban	winter 2013	1.52	0.47	1.79	Hu et al.2017
		summer 2011	1.61	0.56	1.91	
		winter 2010	1.65	0.32	1.58	Hu et al.2016a
Xi'An	urban	summer 2019	1.64	0.58	1.96	Duan et al. 2020
		Before G20		1.78	0.39	1.69
Hangzhou	urban	During G20	1.65	0.58	2.03	Li et al., 2017
		After G20		1.69	0.51	1.84
Lanzhou	urban	winter 2014	1.55	0.28	1.51	
		summer 2012	1.49	0.33	1.58	Xu et al., 2016
Guangzhou	suburban	winter 2014 Nov.	1.63	0.53	1.87	
		winter 2014 Dec.	1.65	0.53	1.87	Qin et al., 2017
Kaiping	suburban	autumn 2008	1.64	0.6	1.94	Huang et al.,2011
Heshan	suburban	autumn 2010	1.65	0.51	1.83	Gong et al., 2012
Shenzhen	urban	winter 2009	1.83	0.39	1.71	He et al.,2011
		summer 2011	1.74	0.45	1.81	Gong et al., 2012
Shanghai	urban	summer 2010	1.92	0.4	1.69	Huang et al.,2012
Ziyang	suburban	winter 2013	1.56	0.65	2.02	Hu et al.2016b
Jiaxing	suburban	summer 2010	1.94	0.36	1.67	
		winter 2010	1.73	0.43	1.75	Huang et al.,2013
HKUST	suburban	summer 2011	1.48	0.64	1.93	
		winter 2012	1.53	0.53	1.8	Li et al., 2015
MongKoK	urban	summer 2013	1.83	0.26	1.5	lee et al., 2015
Fresno.CA (US)	urban	winter 2010	1.75	0.35	1.63	Ge et al. (2012)
Riverside,CA (US)	urban	summer 2005	1.71	0.44	1.73	Docherty et al. (2011)
Korea	urban	winter 2019	1.79	0.37	1.67	Kim et al. 2017
		No BB		1.48	0.84	2.26
Oregon (US)	BB infl	summer 2013	1.49	0.77	2.16	Zhou et al., 2017
			1.53	0.69	2.06	

49

50

51



52

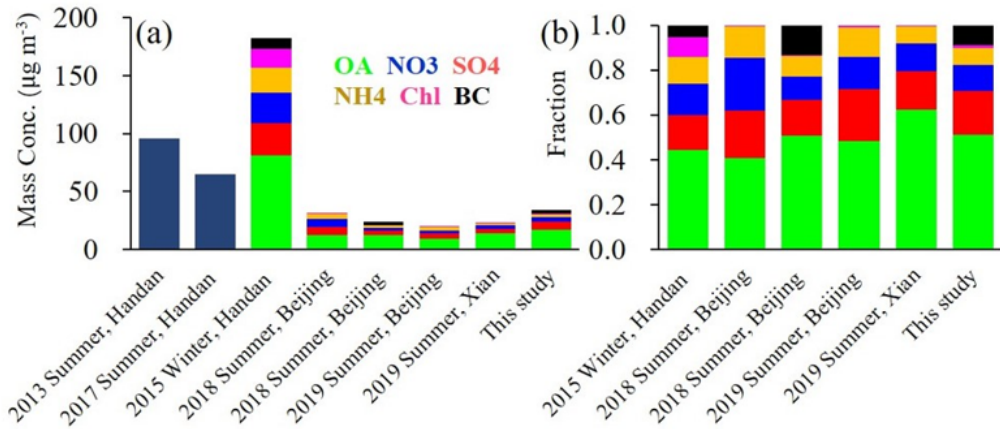
53 **Fig. S1** Location of the PM<sub>2.5</sub> sampling site in Handan (the red star). The base map image was derived  
 54 from AutoNavi Maps (Image © 2022 AutoNavi-GS).

55

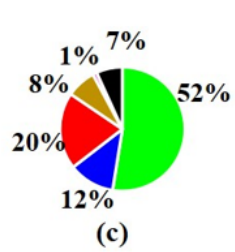
56

57

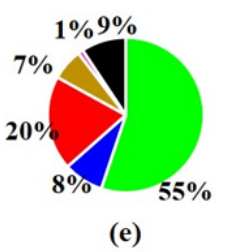
58 .



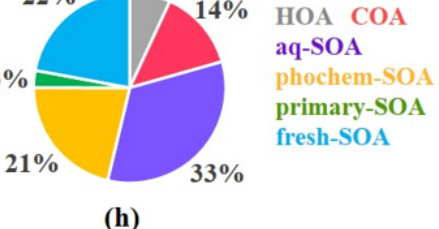
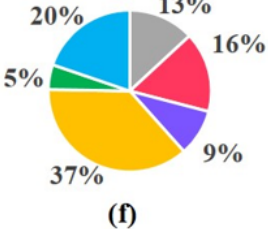
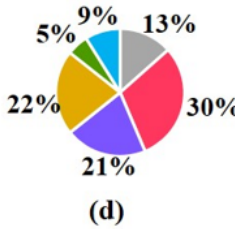
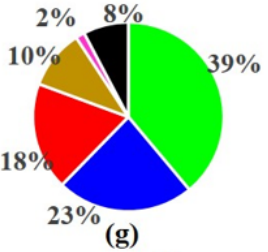
**P1:**  $29.3 \mu\text{g m}^{-3}$



**P2 :**  $36.0 \mu\text{g m}^{-3}$

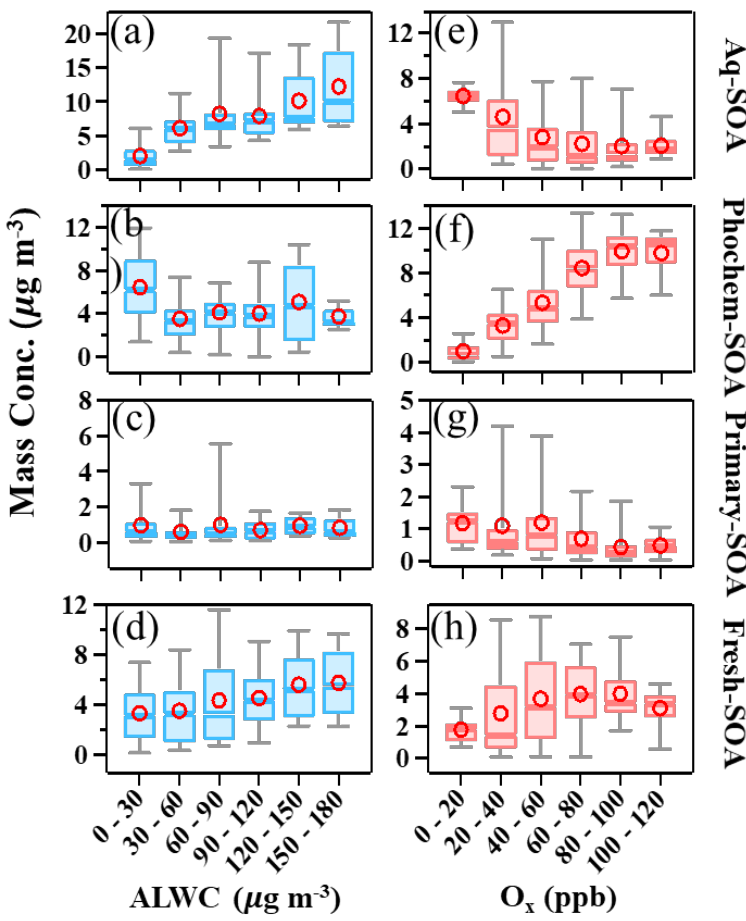


**P3 :**  $63.7 \mu\text{g m}^{-3}$



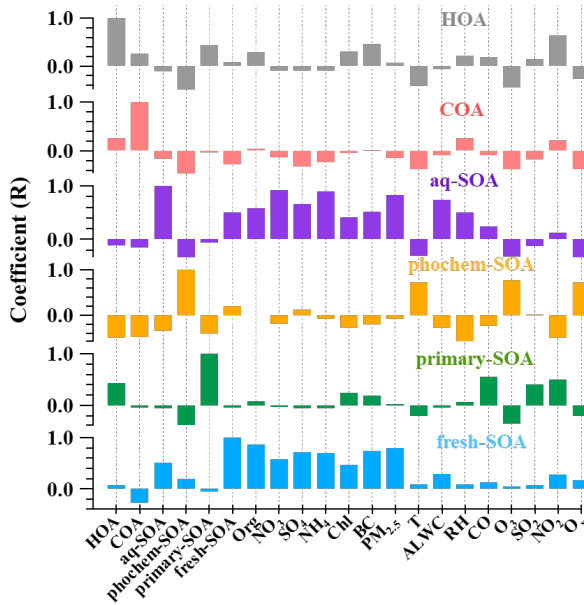
59

60 **Fig. S2** Concentrations (a) and fractions (b) of main chemical components in PM<sub>1</sub>/PM<sub>2.5</sub> during summer  
61 and winter observations in NCP in recent years. The data and references are available in Table S2 of the  
62 Supplement. Fractions of main chemical components of PM<sub>2.5</sub> and OA in reference events (P1: c & d),  
63 high O<sub>x</sub> period (P2: e & f) and high RH period (P3: g & h).



64

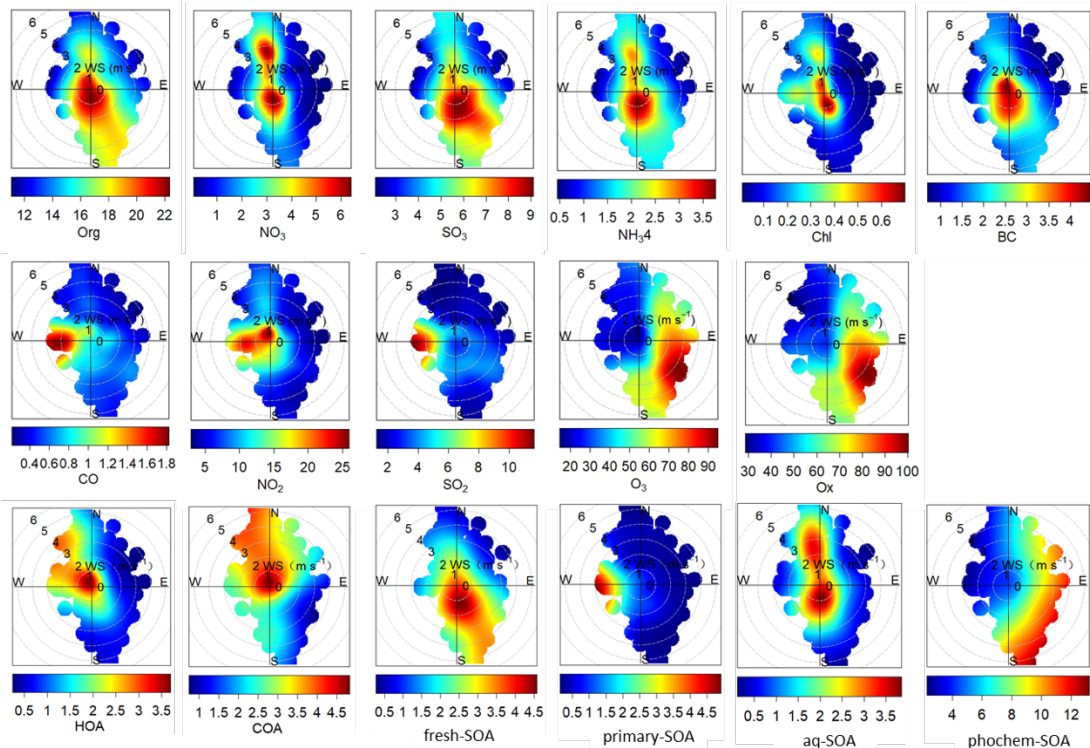
65 **Fig. S3** Variations of the mass concentrations of aq-SOA, phochem-SOA, primary-SOA and fresh-SOA  
 66 as functions of ALWC (a~d) and O<sub>x</sub> (e~h). The data were binned according to the ALWC (30  $\mu\text{g m}^{-3}$   
 67 increment) or O<sub>x</sub> concentration (10 ppb increment), and mean (circle), median (horizontal line), 25th and  
 68 75th percentiles (lower and upper box), and 10th and 90th percentiles (lower and upper whiskers) are  
 69 showed for each bin.



70

71 **Fig. S4** Correlation between the resolved OA factors and other chemical components in  $\text{PM}_{2.5}$ , gas-  
 72 phase pollutants, and meteorological parameters.

73



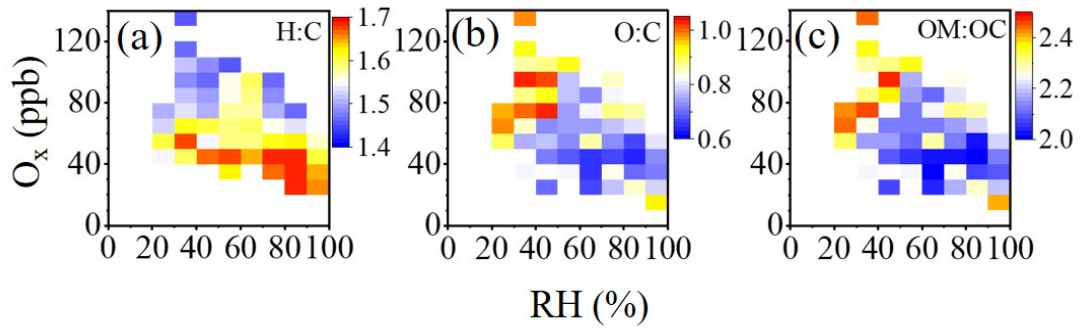
74

75

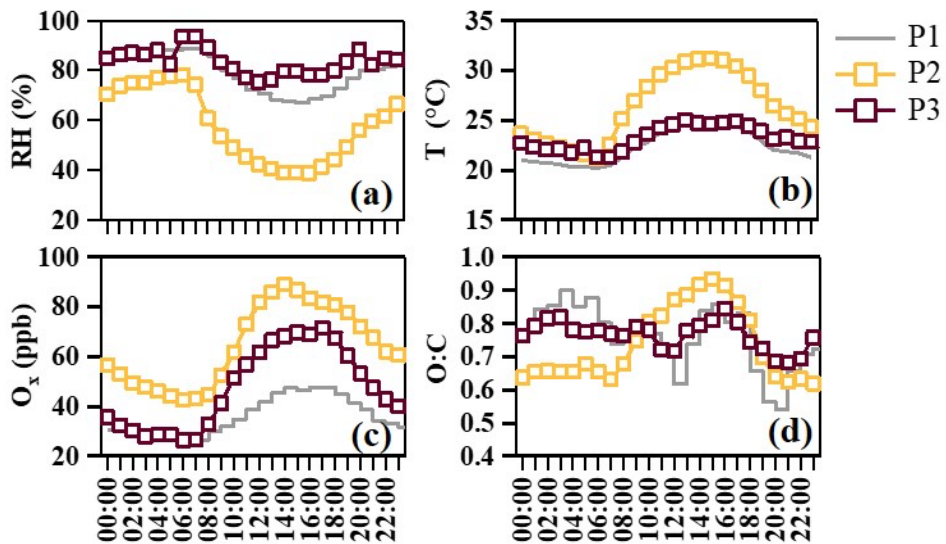
76 **Fig. S5** Polar plots that illustrate the variations of the hourly averaged concentrations of gases pollutants,  
 77  $\text{PM}_{2.5}$  species and OA sources as a function of wind speed ( $\text{m s}^{-1}$ ) and wind direction (°).

78

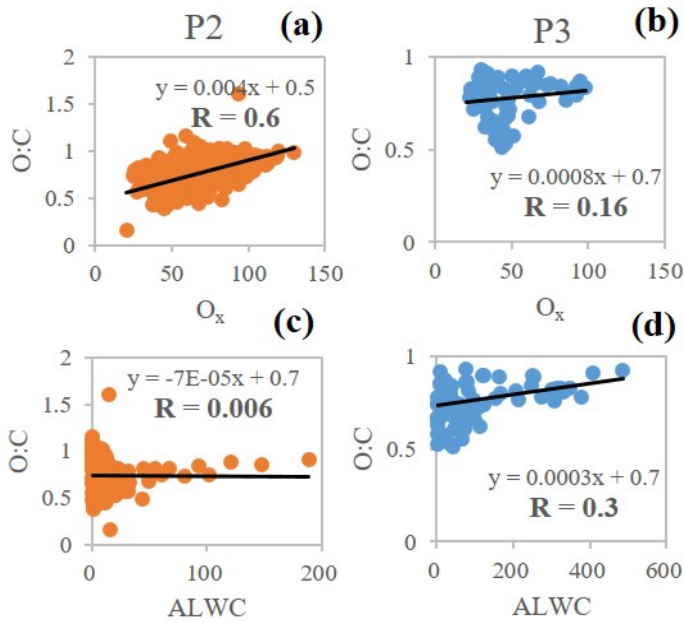
79



80  
81  
82 **Fig. S6** RH- and O<sub>x</sub>-dependent distributions of (a) H:C, (b) O:C and (c) OM:OC ratios. Grids with the  
83 number of points less than five were excluded.  
84



85  
86 **Fig. S7** Diurnal patterns of (a) RH, (b) temperature, (c) O<sub>x</sub> and (d) O:C ratios in reference events (P1),  
87 high O<sub>x</sub> period (P2) and high RH period (P3).  
88



89

90 **Fig. S8** Relationship between O:C ratios and O<sub>x</sub>/ALWC in high O<sub>x</sub> period (P2: a & c) and high  
91 RH period (P3: b & d) during this campaign.

92

93

#### 94 **Supplementary information**

##### 95 **1.1**

96 In the studied time period, POA ( $6.1 \pm 3.61 \mu\text{g m}^{-3}$ ) contributed 30.6% to the bulk OA, including the  
97 hydrocarbon-like OA (HOA, 12.2%) and cooking OA (COA, 19.1%) in summer of Handan. The results  
98 are consistent with the results in summer 2017 and 2018 from Beijing (Xu et al 2019b).

##### 99 **HOA**

100 The spectrum of HOA is substantially contributed by alkyl fragments ( $\text{C}_n\text{H}_{2n+1}^+$  and  $\text{C}_n\text{H}_{2n-1}^+$ , Fig. 1),  
101 major ions include  $\text{C}_3\text{H}_7^+$ ,  $\text{C}_4\text{H}^{9+}$ , and  $\text{C}_5\text{H}_{11}^+$  (Zhao et al., 2019; Xu et al., 2019a; Sun et al., 2016; Elser  
102 et al., 2016; Zhang et al., 2014; Ng et al., 2011), which is consistent with the previous studies  
103 (Canagaratna et al., 2004; Ng et al., 2010). HOA had a relative low O:C ratio of 0.14 and high H:C ratio  
104 of 1.77. On average, it accounted for 12.2% of total OA (Fig. S2a) in Handan, with the absolute  
105 concentration of  $2.4 \pm 2.1 \mu\text{g m}^{-3}$ , which was two times lower than that in Beijing (35%) at the same time  
106 period of 2018 (Chen et al., 2020a). The low HOA fraction was consistent with previous study, which  
107 revealed that transportation was a minor source of atmospheric particles in Handan compared to Beijing  
108 (Wang et al., 2014).

109 High correlations were also observed between the time series of HOA with BC ( $R=0.5$ ) and NO<sub>2</sub> ( $R=0.6$ ,  
110 Fig. S4), supporting the vehicle emission related origins of HOA reported in the previous studies (Lanz  
111 et al., 2007; Docherty et al., 2011). The polar plots (Fig. S5) demonstrated higher concentrations of HOA

112 under relatively low WS ( $< 2.0 \text{ m s}^{-1}$ ), which was very similar with BC, supporting the fact that HOA is  
113 a freshly locally-emitted vehicle OA. HOA exhibited slightly enhanced peaks in the morning (6:00-7:00  
114 local time, LT) and prominent peaks during nighttime (19:00-22:00 LT) when the traffic jam happened  
115 (Fig. 6). However, these kinds of variations were less pronounced in P1 and P3 (Fig. 6), which might  
116 because the high WS and RH had influence to such local sources. Hence the stagnant meteorological  
117 conditions would result in accumulation of local sources during this measurement period. It should be  
118 noted that the fraction of HOA is lower during P3 (7%) compared with P1 and P2, this may be attributed  
119 to the large fraction of SOA (Fig. S2). The average HOA/BC ratio was 0.8, close to other cities in China  
120 e.g., Xianghe (0.91) (Sun et al., 2016), which was between those for diesel trucks (0.5) (Ban-Weiss et  
121 al., 2008) and light-duty vehicles (1.4).

## 122 COA

123 The COA mass spectrum was characterized by higher ratio than HOA between  $f_{55}$  ( $\text{C}_4\text{H}_7^+ + \text{C}_3\text{H}_3\text{O}^+$ ) and  
124  $f_{57}$  ( $\text{C}_4\text{H}_9^+ + \text{C}_3\text{H}_5\text{O}^+$ ) (Mohr et al., 2012), and the spectral pattern was relatively constant among different  
125 years. The O:C and H:C ratios of COA were 0.18 and 1.57, respectively, suggesting their primary feature  
126 (Xu et al., 2016). On average, the mass contribution of COA to OA was 19.1% (Fig. S2a), which was  
127 close to that in the summer of 2018 (15%) in Beijing (Xu et al., 2019b).

128 The most pronounced feature of COA (Fig. 6) is its clearly enhanced diurnal peaks around morning  
129 (6:00–7:00), noon (12:00–13:00) and late evening (19:00–20:00), corresponding to the common meal  
130 hours which was consistent with previous studies of other regions of NCP (Sun et al., 2016; Sun et al.,  
131 2018;). During these meal hours, COA account for over 20% ~ 30% of total OA (Fig. S2d), signifying  
132 the importance of cooking sources in aerosol mass concentrations in urban areas of China.

133 Note that during the different periods, this mass fractions of COA to total OA present stable trend  
134 (14~16%) during P2 and P3, indicating that cooking styles remained consistent and local accumulation  
135 was not the major haze source during the measurement period (Fig. S2). While during the clean periods  
136 of P1 with wind, it increased to 30%, which was the largest contributor to OA. Moreover, the diurnal  
137 pattern of COA show very similar variations from three periods (Fig. 6) with the highest mass  
138 concentration during P1. This significant increase of COA is probably associated with the wind from  
139 southwestern where more residential areas with enhanced domestic cooking activities.

## 140 1.2

### 141 Characteristics of SOA sources

142 SOA accounted for 68.7% to total OA, four SOA factors were resolved depending on the oxidation state,  
143 which correspond to aged SOA and fresh SOA respectively (Jimenez et al., 2009). One factor is attributed  
144 to aqueous-phase chemistry (aq-SOA) and the other to photo-oxidation chemistry (phochem-SOA),  
145 while fresher factor is produced by fresh-source (fresh-SOA), and the other considered as oxidized

146 primary sources denoted as primary-SOA. Although all of the SOA factors were characterized by higher  
147  $m/z$  44 ( $\text{CO}_2^+$ ) and  $m/z$  28 ( $\text{CO}^+$ ) signal, their mass spectrum and temporal trends were noticeably  
148 distinguishable, corresponding to different formation mechanism, which will be discussed in the  
149 following section.

150 **aq-SOA**

151 The aq-SOA was identified as it increased with ALWC but decreased with  $\text{O}_x$  (Fig. S3), which might be  
152 produced in the aqueous-phase events and influenced by aqueous-phase chemistry. The aq-SOA exhibits  
153 the highest O:C ratios of all factors (0.7) and a higher  $f_{\text{CO}_2^+}$  to the total signal of 21.7%, but a low H:C  
154 ratio of 1.24 (Fig. 1). On average, the mass concentration of aq-SOA consisted 15.2% of the total OA  
155 and 22.1% of the SOA (Fig. S2a, b). Good correlations were found between aq-SOA and nitrate ( $R=0.9$ ),  
156 as well as ammonium ( $R=0.9$ , Fig. S4) (Zhang et al., 2007; Aiken et al., 2009 and Huang et al., 2010).  
157 The high correlation with nitrate may be attributed to their similar precursors and formation pathways. It  
158 is also clear that their polar plot patterns are similar (Fig. S5) with two originations of nitrate and aq-  
159 SOA were observed in our study. Results showed that the local origination associated with low wind  
160 speed ( $< 1.0 \text{ m s}^{-1}$ ) had a high concentration up to  $4 \text{ } \mu\text{g m}^{-3}$ , and the regional origination was associated  
161 with relatively high wind speed ( $> 2.5 \text{ m s}^{-1}$ ) derived from the northern regions (Fig. S5), suggesting that  
162 there were mixing regional and local sources for nitrate and aq-SOA. This supports the aq-SOA is  
163 relatively aged in ambient air and influenced by the combination of local formation and regional transport  
164 (Lanz et al., 2007; Hayes et al., 2013; Chen et al., 2021).

165 The aq-SOA contributed a major fraction of 33.3 % to the total OA during P3 (peak concentration:  
166  $25.2 \text{ } \mu\text{g m}^{-3}$ ; peak fraction: 65.3%), pointing the faster SOA production through aqueous-phase chemistry  
167 during this specific haze event compared to P1 (20.5%) and P2 (9.4%). In addition, the ALWC and aq-  
168 SOA were strongly correlated ( $R=0.7$ , Fig. S4), and both were shown dramatically enhancement during  
169 P3 event. This indicates that aq-SOA was either formed via aqueous phase reactions or  
170 absorbed/dissolved into aerosol liquid water. Previous studies also showed that high RH in summer  
171 facilitated the transformation of  $\text{HNO}_3$  into aqueous-phase and increased nitrate concentrations  
172 substantially (Sun et al., 2013; Sun et al., 2015). Due to the high  $\text{NO}_2$  concentration and high RH in this  
173 period, particulate nitrate was produced during this regional transport homogeneously and/or  
174 heterogeneously, resulting in water uptake and high LWC in the aerosol phase. The high ALWC in turn  
175 facilitated further heterogeneous formation of nitrate. This positive feedback provided favorable  
176 conditions for efficient aqueous chemistry and thus production of aq-SOA (Kuang et al., 2020). Note  
177 that the strong correlation between aq-SOA and ALWC was not driven solely by P3 event, rather, the  
178 two time series were remarkably well correlated throughout the entire campaign. This further supported  
179 the interpretation of aq-SOA as characteristic of aqueous SOA production throughout the campaign,  
180 rather than being characteristic of only a single event.

181 **phochem-SOA**

182 The phochem-SOA presented an opposite trend with significant increase as  $O_x$  but decrease as ALWC  
183 (Fig. S3).  $O_x$  has been shown to be a conserved tracer to represent photo-oxidation chemistry (Xu et al.,  
184 2017). The relationship between  $O_x$  and photochemical SOA can offer insight into the formation  
185 mechanism of SOA associated with ozone production chemistry (Herndon et al., 2008). Therefore, when  
186 the mass concentration of phochem-SOA showed a substantial increase as a function of  $O_x$ , it could be  
187 likely due to the enhanced secondary transformation went from less oxidized to more aged with the  
188 progression of atmospheric photochemical aging, which were supported by the large  $O_3$  fractions in  $O_x$   
189 in summertime (Zhang et al., 2019). Such conclusions were further supported by tightly tracked time  
190 series of phochem-SOA with  $O_3$  ( $R = 0.8$ ) and  $O_x$  ( $R = 0.7$ ) (Fig. S4). Considering  $O_3$  has become the  
191 primary air pollutant in summertime in the NCP and had caused the enhancement of atmospheric  
192 oxidation capacity (Chen et al., 2020b), the photochemical processing driven by  $O_3$  might play an  
193 important role in the formation of phochem-SOA.

194 The phochem-SOA had the highest average mass concentration of  $6.1 \pm 3.3 \mu\text{g m}^{-3}$  among the OA  
195 factors, with the highest contribution to total OA (31%) and the SOA (45%) during observation time,  
196 suggesting the predominate role of this factor (Fig. S2). The phochem-SOA was oxidized with an O:C  
197 ratio of 0.67 and H:C ratio of 1.18, and it also had high  $\text{CO}_2^+$  contribution of 17.9 %, which further  
198 suggested that the atmospheric oxidation capacity during summer was strong. Similar to aq-SOA,  
199 phochem-SOA also showed large variations during different periods. It accounted the most of 36.9% to  
200 OA during P2, compared to other two periods (21.5% in P1 and 21.3% in P3, respectively), indicating  
201 that the enhancement of phochem-SOA can leads to the development of SOA formation. The phochem-  
202 SOA also had the similar spatial pattern with  $O_3$  and  $O_x$  form the polar plots (Fig. S5), where high  
203 concentration associated with southeast wind originated from Shandong with relatively high wind speed  
204 of over  $4 \text{ m s}^{-1}$ , suggesting the typical feature of regional transport pollutants.

205 **primary-related-SOA**

206 In terms of two fresh SOA factors, they were defined as less oxidized OOA by relative lower O:C,  
207 stronger intensity of  $m/z$  43 (mainly  $\text{C}_2\text{H}_3\text{O}^+$ ) and  $m/z$  44 (mainly  $\text{CO}_2^+$ ).

208 The primary-SOA constituted the lowest contribution of 5% among all factors of the total OA and 7%  
209 of the SOA, however, it is still of particular interest in this study. It is characterized by both lower H:C  
210 (1.09) and O:C (0.54) ratios with  $\text{CO}_2^+$  comprising 14.3%, which are higher than other POA factors,  
211 indicating a typical nature of less oxidized SOA. However, at  $m/z > 120$ , clear polycyclic aromatic  
212 hydrocarbons (PAHs) fragments are evident in mass spectrum of primary-SOA (Fig. 1), as indicated by  
213 the presence of similar patterns of PAH-like ions in their mass spectra at  $m/z$  152, 165, 178, 189, 202,  
214 216, 226 + 228, 240 + 242, 250 + 252, 264 + 266 and 276 + 278 (Dzepina et al., 2007). Previous AMS  
215 studies have observed pronounced peaks of PAHs ions in POA spectrum, such as CCOA (coal

216 combustion) and BBOA (biomass burning) (Hu et al., 2016a; Zhao et al., 2019), but rarely in SOA. This  
217 observation implies that Primary-SOA may be link to the POA origin from domestic coal combustion  
218 (Xu et al., 2006). Through laboratory combustion studies using online aerosol mass spectrometry, they  
219 examined substantial ion signal at  $m/z > 100$ , which potentially link to the fragments of high molecular  
220 weight (HMW) species, was pronounced in both oxidized POA (OPOA) and POA, indicating that POA  
221 can be oxidized by multiphase reactions forming OPOA and the degradation of HMW species from the  
222 oxidation process (Budisulistiorini et al., 2021). In our study, the similar signatures of PAH-like ions was  
223 also found in aq-SOA at  $m/z > 150$ , but less pronounced in aq-SOA compared to Primary-SOA,  
224 consistent with previous study in Beijing (Wang et al., 2021). The observation of PAH-likes ions in both  
225 primary-SOA and aq-SOA further indicated they might both originated from coal combustion or  
226 transformation by oxidized POA, and the oxidation of PAHs being involved in the conversion of  
227 Primary-SOA to aq-SOA.

228 As it is shown in Fig. S4, primary-SOA exhibited relative better correlations with some gaseous  
229 pollutants, such as CO ( $R = 0.6$ ), NO<sub>2</sub> ( $R = 0.5$ ), and was also consistent with the temporal pattern of  
230 HOA ( $R = 0.4$ ), suggesting primary-SOA might be transformed from locally primary emissions. In  
231 addition, primary-SOA, had no significant increase trend with both ALWC and O<sub>x</sub> (Fig. S3), but its  
232 pollution pattern was similar as some primary precursors such as CO, SO<sub>2</sub> and NO<sub>2</sub>, where higher  
233 concentrations appeared with weak west wind (Fig. S5). Therefore, the major pathway of this primary-  
234 SOA formation might be related to primary emission or the its transformation, which also supported by  
235 similar results obtained by Rivellini et al., (2020), who found the oxygenated part of combustion particles  
236 which was co-emitted with HOA and/or produced by oxidation of HOA rapidly could be oxygenated-  
237 HOA (O-HOA) or oxygenated-CCOA. Moreover, some SOA factors were defined as “urban-lifestyle  
238 SOAs” because it could derived from some POA exhaust such as vehicle and cooking through laboratory  
239 experiments (Zhang et al., 2021).

#### 240 **fresh-SOA**

241 The fresh-SOA showed increase substantially as ALWC increasing, similar to aq-SOA. Whereas it also  
242 showed slight increase trend following O<sub>x</sub> when O<sub>x</sub> < 100 ppb (Fig. S3). Therefore, both aqueous-phase  
243 chemistry and photochemical processing were thought to have positive impacts synchronously on  
244 formation of Fresh-SOA. In this study, CO<sub>2</sub><sup>+</sup> comprised at least in Fresh-SOA of 8.3%, corresponding  
245 with the lowest atomic O:C ratio of 0.41 and a highest atomic H:C ratio of 1.41 among the four SOA  
246 factors. These characteristics consistent with the global average of LO-OOA of 0.35 ± 0.14, Ng et al.,  
247 2010), demonstrating the it is more fresh SOA. Besides, Fig. S2 showed that fresh-SOA consisted 18%  
248 of the total OA and 26% of the SOA. Note that the concentration of fresh-SOA increased in every event  
249 following with OA increased no matter the aqueous-phase event and photochemical event under the  
250 stagnant conditions. Meanwhile, it was well correlated with total OA ( $R = 0.9$ ), PM<sub>2.5</sub> ( $R = 0.8$ ) and BC  
251 ( $R = 0.7$ , Fig. S4), as well as sulfate ( $R = 0.7$ ). The sustained contribution from fresh-SOA and

252 covariations between fresh-SOA with these species suggest that it was probably a mixed source which  
253 not just dominantly driven by only one formation mechanism. Nevertheless, different pathways among  
254 P1, P2 and P3 lead to the progressive fractions of fresh-SOA to total OA. Compared with P1,  
255 photochemical processing (P2) and aqueous-phase reactions (P3) strengthen to produce fresh-SOA  
256 individually, but the influence driven by aqueous-phase reactions is much greater than photochemical  
257 processing.

### 258 **1.3 Evolution of OA**

259 The mass spectra of these four factors for PM<sub>2.5</sub> are dominated by *m/z* 44 (mainly CO<sub>2</sub><sup>+</sup>) (Fig. 1).  
260 However, their concentrations show very different temporal variations. The concentration of aq-SOA  
261 correlates with NO<sub>3</sub> (*R* = 0.9) and ALWC (*R* = 0.7), showing a steady increase as a function of ALWC  
262 (Fig. S4 and Fig. S3) which might indicate aqueous-phase chemistry. The aq-SOA exhibits the highest  
263 O:C ratio of all factors (0.7) and more aged oxidation state, while the O:C ratio of phochem-SOA remains  
264 high (0.67) but slightly lower compared to aq-SOA. The phochem-SOA presents an opposite trend with  
265 significant increase as function of O<sub>x</sub> but decrease as function of ALWC (Fig. S3), suggesting the  
266 photochemical formation and further supported by tightly tracked time series of phochem-SOA with O<sub>3</sub>  
267 (*R* = 0.8) and O<sub>x</sub> (*R* = 0.7) (Fig. S4). The mass spectrum of the fresh-SOA shows a high peak at *m/z* 43  
268 (mainly C<sub>2</sub>H<sub>3</sub>O<sup>+</sup>) (Fig. 1), corresponding to the lowest atomic O:C ratio of 0.41 and a highest atomic H:C  
269 ratio of 1.41 among SOA factors, which indicate its feature of fresher SOA. Note that the concentration  
270 of fresh-SOA increased in every period with OA increase, and was well correlated with total OA (*R* =  
271 0.9), PM<sub>2.5</sub> (*R* = 0.8) and BC (*R* = 0.7), as well as SO<sub>4</sub> (*R* = 0.7) (Fig. S4), indicating that they were  
272 freshly emitted and less oxidized. The primary-SOA in this study was of particular interest. It has  
273 relatively low O:C (0.54) and H:C (1.09) ratios, indicating a typical nature of less oxidized SOA.  
274 However, as shown in Fig. S4, primary-SOA exhibits relative better correlations with some gaseous  
275 pollutants, such as CO (*R* = 0.6), NO<sub>2</sub> (*R* = 0.5), and was also consistent with the temporal pattern of  
276 HOA (*R* = 0.4), suggesting primary-SOA might be transformed from locally primary emissions.

### 277 **1.4 VK Diagram**

278 During this campaign, the H:C and O:C ratios in this study showed little variation, with average values  
279 of 0.75 ± 0.09 and 1.58 ± 0.28, respectively (Fig. 8a). The H:C ratio in Handan was slightly higher than  
280 that in Hong Kong (1.48) and Lanzhou (1.49) but lower than those at urban sites in Shenzhen (1.83),  
281 MongKok (1.83), Shanghai (1.92) and Jiaxing (1.94) (He et al., 2011; Huang et al., 2012, 2013; Li et al.,  
282 2015; Lee et al., 2015; Xu et al., 2016). Also, a general consistency was observed for the O:C ratio which  
283 was higher than mostly other sites, except the site in Oregon (US) influenced by wildfire. Overall, this  
284 relatively low H:C ratio, high O:C ratios suggested that OA in summer of Handan had higher degree of  
285 oxygenation than those at urban sites due to the progress of atmospheric photochemical aging, and also  
286 indicated the secondary portion having a substantial contribution to the bulk OA. Figure S5 shows a

287 synergistically impact of RH and O<sub>x</sub> to elemental ratios. For example, H:C increased with the decrease  
288 of O<sub>x</sub> concentration and with the increase of RH, which indicated that photochemical process had a  
289 positive effect but aqueous-phase process had an opposite effect on the H:C of atmospheric O. As for  
290 O:C, higher O:C ratio was mainly observed with high concentration of O<sub>x</sub>, highlighting the importance  
291 of photochemical process in aerosol oxidation during summer. Meanwhile, slightly higher O:C also  
292 occurred at high RH levels even though the low concentration of O<sub>x</sub>. Previous studies have demonstrated  
293 that aqueous-phase reactions of low-volatility high-molecular weight species detected in the atmosphere,  
294 such as glyoxal (Waxman et al., 2013), methylglyoxal (Lim et al., 2013), glycolaldehyde (Schöne and  
295 Herrmann, 2014), pyruvic acid (Altieri et al., 2006), and methacrolein (Liu et al., 2012), were the  
296 important formation pathway of OA (Kroll and Seinfeld, 2008; Hallquist et al., 2009; Sun et al., 2010;  
297 Chen et al., 2018). The products, such as highly oxygenated organic molecules (HOMs), from these  
298 aqueous-phase reactions would be conducive to elevating O:C (Molteni et al., 2018; Bianchi et al., 2019).  
299 On the other hand, the Fig. S7 showed that, the O:C ratio generally increased and the H:C ratio decreased  
300 during the day of 8:00–16:00 local time (LT), suggesting that SOA formation like photochemical process  
301 or mixing with more aged aerosols from regional sources was dominant during the day and outweighed  
302 the emissions POA (Sun et al., 2013).

303 To further investigate the pathways of OA factors, ions in the HR mass spectra were used to calculate  
304 the elemental ratios using the improved-ambient method (Canagaratna et al., 2015). The ratios were  
305 represented by the VK diagram in Fig. 8a (Heald et al., 2010) to show the OA evolution in the  
306 summertime of Handan. Based on our data, we found that HOA and COA factors (POA) are both located  
307 at the left-top corner with high H:C, low O:C and OSc below -1. Then, these POAs evolve toward the  
308 right bottom during the formation of SOA (Zhao et al., 2019). Functional groups are further added in Fig.  
309 8a: only oxygen atoms to a carbon backbone results in a slope equal 0, while the replacement of a  
310 hydrogen atom with a carboxylic acid group (-COOH) results in a slope of -1 without fragmentation  
311 (Heald et al., 2010; Ng et al., 2011). As organic compounds are oxidized, a relatively flat slope of -0.19  
312 for H:C versus O:C in this study suggests the importance of the addition of alcohol and/or peroxide (slope  
313 = 0) in OA aging with additional processes adding carboxylic acid and/or carboxyl groups. For SOA  
314 factors, Fresh-SOA factors are located in upper left region with high H:C and low O:C values compared  
315 with the other SOA factors. Although the primary-SOA has the lower O:C than other SOAs, it still  
316 located closely to these two SOAs, which further indicates they might have similar formation,  
317 compositions or transformation between these factors, which is consistent with the results from above  
318 section.

319 Table S3 present the comparison of average O:C ( $0.77 \pm 0.1$ ) and H:C ( $1.58 \pm 0.1$ ) for bulk OA in this  
320 study (three periods in Handan) with studies from China and other campaigns (four seasons in  
321 urban/suburban sites) based on the updated IA calibrations in Canagaratna et al. (2015). Briefly, OA in  
322 this study are at the higher end of O:C ranges reported in urban areas of China, and are comparable to

323 the O:C ratios at the suburban sites, suggesting the OA was fairly oxidized in summer in the urban  
324 Handan.

325 **1.5  $f_{43}$  Versus  $f_{44}$**

326 Since the ion fragment with  $m/z = 44$  and 43 are usually originated from different functional groups and  
327 the ratio changes as a function of atmospheric aging, researchers usually use the triangle plot of  $f_{44}$  versus  
328  $f_{43}$  to characterize OA evolutions in the atmosphere. As shown in Fig. 8b, POA and SOA factors fell into  
329 similar regions of  $f_{44}$  versus  $f_{43}$ , suggesting that OA factors identified by PMF were fairly similar in the  
330 summertime of Handan. The bottom region of the triangle was dominated by POA factors (including  
331 HOA and COA) with low  $f_{44}$  (about 0.05) and  $f_{43}$  of 0.06 to 0.08, indicating that they were freshly emitted  
332 and less oxidized. Comparatively, SOA factors are located in different regions: (1) the fresh-SOA region  
333 with low  $f_{44}$  ( $<0.10$ ), indicating they were relatively less oxidized compared to other SOA factors. (2) the  
334 region with high  $f_{44}$  ( $>0.17$ ) than other OA factors, consistent with the fact that sq-SOA and phochem-  
335 SOA were surrogates of highly oxidized or regionally transported SOAs (Zhao et al., 2019); and (3)  
336 primary-SOA region, showing freshly oxidized properties ( $f_{44}$  around 0.15). From the color plot of  $f_{29}$   
337 (mainly  $f_{\text{CHO}^+}$ ),  $f_{\text{CHO}^+}$  was observed highly correlated with formation of aged SOA factors.

338

339 **References**

340

341 Aiken, A. C., Salcedo, D., Cubison, M. J., Huffman, J. A., DeCarlo, P. F., Ulbrich, I. M., Docherty, K.  
342 S., Sueper, D., Kimmel, J. R., Worsnop, D. R., Trimborn, A., Northway, M., Stone, E. A., Schauer,  
343 J. J., Volkamer, R. M., Fortner, E., de Foy, B., Wang, J., Laskin, A., Shutthanandan, V., Zheng, J.,  
344 Zhang, R., Gaffney, J., Marley, N. A., Paredes-Miranda, G., Arnott, W. P., Molina, L. T., Sosa, G.,  
345 and Jimenez, J. L.: Mexico City aerosol analysis during MILAGRO using high resolution aerosol  
346 mass spectrometry at the urban supersite (T0) – Part 1: Fine particle composition and organic  
347 source apportionment, *Atmos. Chem. Phys.*, 9, 6633–6653, <https://doi.org/10.5194/acp-9-6633-2009>, 2009.

349 Altieri K E, Carlton A G, Lim H J, et al. Evidence for oligomer formation in clouds: Reactions of isoprene  
350 oxidation products. *Environmental science & technology*, 40(16): 4956-4960,  
351 <https://doi.org/10.1021/es052170n>, 2006.

352 Ban-Weiss, G. A., J. P. McLaughlin, R. A. Harley, M. M. Lunden, T. W. Kirchstetter, A. J. Kean, A. W.  
353 Strawa, E. D. Stevenson, and G. R. Kendall, Long-term changes in emissions of nitrogen oxides  
354 and particulate matter from on-road gasoline and diesel vehicles, *Atmos. Environ.*, 42(2), 220-232,  
355 <https://doi.org/10.1016/j.atmosenv.2007.09.049>, 2008.

356 Bianchi F, Kurtén T, Riva M, et al. Highly oxygenated organic molecules (HOM) from gas-phase  
357 autoxidation involving peroxy radicals: A key contributor to atmospheric aerosol. *Chemical  
358 reviews*, 119(6): 3472-3509. DOI: 10.1021/acs.chemrev.8b00395, 2019.

359 Budisulistiorini S H, Chen J, Itoh M, et al. Can Online Aerosol Mass Spectrometry Analysis Classify  
360 Secondary Organic Aerosol (SOA) and Oxidized Primary Organic Aerosol (OPOA)? A Case Study  
361 of Laboratory and Field Studies of Indonesian Biomass Burning. *ACS Earth and Space Chemistry*,  
362 5(12): 3511-3522, <https://doi.org/10.1021/acsearthspacechem.1c00319>, 2021.

363 Canagaratna M R, Jayne J T, Ghertner D A, et al. Chase Studies of Particulate Emissions from in-use  
364 New York City Vehicles, *Aerosol Science and Technology*, 38:6, 555-573, DOI:  
365 10.1080/02786820490465504, 2004.

366 Canagaratna, M.R., Jimenez, J.L., Kroll, J.H., Chen, Q., Kessler, S.H., Massoli, P., Hildebrandt Ruiz, L.,  
367 Fortner, E., Williams, L.R., Wilson, K.R., Surratt, J.D., Donahue, N.M., Jayne, J.T., Worsnop,  
368 D.R., 2015. Elemental ratio measurements of organic compounds using aerosol mass spectrometry:  
369 Characterization, improved calibration, and implications. *Atmos. Chem. Phys.* 15, 253–272.  
370 <https://doi.org/10.5194/acp-15-253-2015>

371 Chen T, Liu J , Liu Y , et al. Chemical characterization of submicron aerosol in summertime Beijing: A  
372 case study in southern suburbs in 2018. *Chemosphere*, 247:125918, 2020a

373 Chen, T., Liu, J., Ma, Q., Chu, B., Zhang, P., Ma, J., Liu, Y., Zhong, C., Liu, P., Wang, Y., Mu, Y., and  
374 He, H.: Measurement report: Effects of photochemical aging on the formation and evolution of  
375 summertime secondary aerosol in Beijing, *Atmos. Chem. Phys. Discuss.*,  
376 <https://doi.org/10.5194/acp-2020-792>, in review, 2020b.

377 Chen, W., Ye, Y., Hu, W., Zhou, H., Pan, T., Wang, Y., Song, W., Song, Q., Ye, C., Wang, C., Wang,  
378 B., Huang, S., Yuan, B., Zhu, M., Lian, X., Zhang, G., Bi, X., Jiang, F., Liu, J., Canonaco, F.,  
379 Prevot, A.S.H., Shao, M., Wang, X., 2021. Real-time characterization of aerosol compositions,  
380 sources and aging processes in Guangzhou during PRIDE-GBA 2018 campaign. *J. Geophys. Res.*  
381 *Atmos.* <https://doi.org/10.1029/2021jd035114>

382 Docherty, K. S., Aiken, A. C., Huffman, J. A., Ulbrich, I. M., DeCarlo, P. F., Sueper, D., Worsnop, D.  
383 R., Snyder, D. C., Peltier, R. E., Weber, R. J., Grover, B. D., Eatough, D. J., Williams, B. J.,  
384 Goldstein, A. H., Ziemann, P. J., and Jimenez, J. L.: The 2005 Study of Organic Aerosols at  
385 Riverside (SOAR-1): instrumental intercomparisons and fine particle composition, *Atmos. Chem.*  
386 *Phys.*, 11, 12387–12420, <https://doi.org/10.5194/acp-11-12387-2011>, 2011

387 Duan, J., Huang, R.-J., Li, Y., Chen, Q., Zheng, Y., Chen, Y., Lin, C., Ni, H., Wang, M., Ovadnevaite,  
388 J., Ceburnis, D., Chen, C., Worsnop, D.R., Hoffmann, T., O'Dowd, C., Cao, J.J., 2020.  
389 Summertime and wintertime atmospheric processes of secondary aerosol in Beijing *Atmos. Chem.*  
390 *Phys.* 20, 3793–3807.

391 Dzepina, K., Arey, J., Marr, L.C., Worsnop, D.R., Salcedo, D., Zhang, Q., Onasch, T.B., Molina, L.T.,  
392 Molina, M.J., Jimenez, J.L., 2007. Detection of particle-phase polycyclic aromatic hydrocarbons  
393 in Mexico City using an aerosol mass spectrometer. *Int. J. Mass Spectrom.* 263, 152–170.  
394 <https://doi.org/10.1016/j.ijms.2007.01.010>

395 Elser, M., Huang, R.-J., Wolf, R., Slowik, J.G., Wang, Q., Canonaco, F., Li, G., Bozzetti, C., Daellenbach,  
396 K.R., Huang, Y., Zhang, R., Li, Z., Cao, J., Baltensperger, U., ElHaddad, I., Prevot, A.S.H., 2016.

397 New insights into PM2.5 chemical composition and sources in two major cities in China during  
398 extreme haze events using aerosol mass spectrometry. *Atmos. Chem. Phys.* 16, 3207–3225.

399 Ge, X. L., Setyan, A., Sun, Y. L., and Zhang, Q.: Primary and secondary organic aerosols in Fresno,  
400 California during wintertime: Results from high resolution aerosol mass spectrometry, *J. Geophys.*  
401 *Res.*, 117, D19301, <https://doi.org/10.1029/2012JD018026>, 2012.

402 Gu, Yifang; Huang, Ru-Jin; Li, Yongjie; Duan, Jing; Chen, Qi; Hu, Weiwei; Zheng, Yan; Lin, Chunshui;  
403 Ni, Haiyan; Dai, Wenting; Cao, Junji; Liu, Quan; Chen, Yang; Chen, Chunying; Ovadnevaite,  
404 Jurgita; Ceburnis, Darius; O'Dowd, Colin. Chemical nature and sources of fine particles in urban  
405 Beijing: Seasonality and formation mechanisms. *Environment International*, 2020, 140. DOI:  
406 10.1016/j.envint.2020.105732

407 Gong, Z., Lan, Z., Xue, L., Zeng, L., He, L., and Huang, X.: Characterization of submicron aerosols in  
408 the urban outflow of the central Pearl River Delta region of China, *Front. Env. Sci. Eng.*, 6, 725-  
409 733, <https://doi.org/10.1007/s11783-012-0441-8>, 2012

410 Hallquist, M., Wenger, J. C., Baltensperger, U., Rudich, Y., Simpson, D., Claeys, M., Dommen, J.,  
411 Donahue, N. M., George, C., Goldstein, A. H., Hamilton, J. F., Herrmann, H., Hoffmann, T.,  
412 Iinuma, Y., Jang, M., Jenkin, M. E., Jimenez, J. L., Kiendler-Scharr, A., Maenhaut, W., McFiggans,  
413 G., Mentel, Th. F., Monod, A., Prévôt, A. S. H., Seinfeld, J. H., Surratt, J. D., Szmigielski, R., and  
414 Wildt, J.: The formation, properties and impact of secondary organic aerosol: current and emerging  
415 issues, *Atmos. Chem. Phys.*, 9, 5155–5236, <https://doi.org/10.5194/acp-9-5155-2009>, 2009.

416 Hayes, P. L., Ortega, A. M., Cubison, M. J., Froyd, K. D., Zhao, Y., Cliff, S. S., Hu, W. W., Toohey, D.  
417 W., Flynn, J. H., Lefer, B. L., Grossberg, N., Alvarez, S., Rappenglück, B., Taylor, J. W., Allan, J.  
418 D., Holloway, J. S., Gilman, J. B., Kuster, W. C., de Gouw, J. A., Massoli, P., Zhang, X., Liu, J.,  
419 Weber, R. J., Corrigan, A. L., Russell, L. M., Isaacman, G., Worton, D. R., Kreisberg, N. M.,  
420 Goldstein, A. H., Thalman, R., Waxman, E. M., Volkamer, R., Lin, Y. H., Surratt, J. D., Kleindienst,  
421 T. E., Offenberg, J. H., Dusanter, S., Griffith, S., Stevens, P. S., Brioude, J., Angevine, W. M., and  
422 Jimenez, J. L.: Organic aerosol composition and sources in Pasadena, California, during the 2010  
423 CalNex campaign, *J. Geophys. Res.-Atmos.*, 118, 9233–9257, <https://doi.org/10.1002/jgrd.50530>,  
424 2013.

425 He, L. Y., Huang, X. F., Xue, L., Hu, M., Lin, Y., Zheng, J., Zhang, R. Y., and Zhang, Y. H.: Submicron  
426 aerosol analysis and organic source apportionment in an urban atmosphere in Pearl River Delta of  
427 China using high-resolution aerosol mass spectrometry, *J. Geophys. Res.*, 116, D12304,  
428 <https://doi.org/10.1029/2010JD014566>, 2011.

429 Heald, C.L., Kroll, J.H., Jimenez, J.L., Docherty, K.S., Decarlo, P.F., Aiken, A.C., Chen, Q., Martin,  
430 S.T., Farmer, D.K., Artaxo, P., 2010. A simplified description of the evolution of organic aerosol  
431 composition in the atmosphere. *Geophys. Res. Lett.* 37. <https://doi.org/10.1029/2010GL042737>

432 Herndon, S.C., Onasch, T.B., Wood, E.C., Kroll, J.H., Canagaratna, M.R., Jayne, J.T., Zavala, M.A.,  
433 Knighton, W.B., Mazzoleni, C., Dubey, M.K., Ulbrich, I.M., Jimenez, J.L., Seila, R., de Gouw,  
434 J.A., de Foy, B., Fast, J., Molina, L.T., Kolb, C.E., Worsnop, D.R., 2008. Correlation of secondary

435 organic aerosol with odd oxygen in Mexico City. *Geophys. Res. Lett.* 35.  
436 <https://doi.org/10.1029/2008GL034058>

437 Hu, J., Wang, P., Ying, Q., Zhang, H., Chen, J., Ge, X., Li, X., Jiang, J., Wang, S., Zhang, J., Zhao, Y.,  
438 Zhang, Y., 2017. Modeling biogenic and anthropogenic secondary organic aerosol in China. *Atmos.*  
439 *Chem. Phys.* 17, 77–92.

440 Hu, W.W., Hu, M., Hu, W., Jimenez, J.L., Yuan, B., Chen, W., Wang, M., Wu, Y., Chen, C., Wang, Z.,  
441 Peng, J., Zeng, L., Shao, M., 2016a. Chemical composition, sources, and aging process of  
442 submicron aerosols in Beijing: Contrast between summer and winter. *J. Geophys. Res.-Atmos.* 121,  
443 1955–1977.

444 Hu, W., Hu, M., Hu, W.-W., Niu, H., Zheng, J., Wu, Y., Chen, W., Chen, C., Li, L., Shao, M., Xie, S.,  
445 and Zhang, Y.: Characterization of submicron aerosols influenced by biomass burning at a site in  
446 the Sichuan Basin, southwestern China, *Atmos. Chem. Phys.*, 16, 13213–13230,  
447 <https://doi.org/10.5194/acp-16-13213-2016>, 2016b

448 Huang, X.-F., He, L.-Y., Hu, M., Canagaratna, M. R., Sun, Y., Zhang, Q., Zhu, T., Xue, L., Zeng, L.-W.,  
449 Liu, X.-G., Zhang, Y.-H., Jayne, J. T., Ng, N. L., and Worsnop, D. R.: Highly timeresolved  
450 chemical characterization of atmospheric submicron particles during 2008 Beijing Olympic Games  
451 using an Aerodyne High-Resolution Aerosol Mass Spectrometer, *Atmos. Chem. Phys.*, 10, 8933–  
452 8945, <https://doi.org/10.5194/acp-10-8933-2010>, 2010.

453 Huang, X.-F., He, L.-Y., Hu, M., Canagaratna, M. R., Kroll, J. H., Ng, N. L., Zhang, Y. H., Lin, Y., Xue,  
454 L., Sun, T. L., Liu, X. G., Shao, M., Jayne, J. T., and Worsnop, D. R.: Characterization of  
455 submicron aerosols at a rural site in Pearl River Delta of China using an Aerodyne HighResolution  
456 Aerosol Mass Spectrometer, *Atmos. Chem. Phys.*, 11, 1865-1877, <https://doi.org/10.5194/acp-11-1865-2011>, 2011.

458 Huang, X.-F., He, L.-Y., Xue, L., Sun, T.-L., Zeng, L.-W., Gong, Z.-H., Hu, M., and Zhu, T.: Highly  
459 time-resolved chemical characterization of atmospheric fine particles during 2010 Shanghai World  
460 Expo, *Atmos. Chem. Phys.*, 12, 4897–4907, <https://doi.org/10.5194/acp-12-4897-2012>, 2012.

461 Huang, X.-F., Xue, L., Tian, X. D., Shao, W. W., Sun, T. L., Gong, Z. H., Ju, W. W., Jiang, B., Hu, M.,  
462 and He, L. Y.: Highly time-resolved carbonaceous aerosol characterization in Yangtze River Delta  
463 of China: Composition, mixing state and secondary formation, *Atmos. Environ.*, 64, 200–207,  
464 <https://doi.org/10.1016/j.atmosenv.2012.09.059>, 2013

465 Jimenez, J.L., Canagaratna, M.R., Donahue, N.M., Prevot, A.S.H., Zhang, Q., Kroll, J.H., DeCarlo, P.F.,  
466 Allan, J.D., Coe, H., Ng, N.L., Aiken, A.C., Docherty, K.S., Ulbrich, I.M., Grieshop, A.P.,  
467 Robinson, A.L., Duplissy, J., Smith, J.D., Wilson, K.R., Lanz, V.A., Hueglin, C., Sun, Y.L., Tian,  
468 J., Laaksonen, A., Raatikainen, T., Rautiainen, J., Vaattovaara, P., Ehn, M., Kulmala, M.,  
469 Tomlinson, J.M., Collins, D.R., Cubison, M.J., Dunlea, J., Huffman, J.A., Onasch, T.B., Alfarra,  
470 M.R., Williams, P.I., Bower, K., Kondo, Y., Schneider, J., Drewnick, F., Borrmann, S., Weimer,  
471 S., Demerjian, K., Salcedo, D., Cottrell, L., Griffin, R., Takami, A., Miyoshi, T., Hatakeyama, S.,  
472 Shimono, A., Sun, J.Y., Zhang, Y.M., Dzepina, K., Kimmel, J.R., Sueper, D., Jayne, J.T., Herndon,  
473 S.C., Trimborn, A.M., Williams, L.R., Wood, E.C., Middlebrook, A.M., Kolb, C.E., Baltensperger,

474 U., Worsnop, D.R., 2009. Evolution of Organic Aerosols in the Atmosphere. *Science*. 326(5959),  
475 1525–1529.

476 Kroll, J.H., Seinfeld, J.H., 2008. Chemistry of secondary organic aerosol: formation and evolution of  
477 low-volatility organics in the atmosphere. *Atmos. Environ.* 42, 3593-3624.

478 Kuang, Y., He, Y., Xu, W.Y., Yuan, B., Zhang, G., Ma, Z.Q., Wu, C.H., Wang, C.M., Wang, S.H., Zhang,  
479 S.Y., Tao, J.C., Ma, N., Su, H., Cheng, Y.F., Shao, M., Sun, Y.L., 2020. Photochemical aqueous-  
480 phase reactions induce rapid daytime formation of oxygenated organic aerosol on the North China  
481 Plain. *Environ. Sci. Technol.* 54(7), 3849–3860.

482 Lanz, V. A., Alfarra, M. R., Baltensperger, U., Buchmann, B., Hueglin, C., and Prévôt, A. S. H.: Source  
483 apportionment of sub- micron organic aerosols at an urban site by factor analytical mod- elling of  
484 aerosol mass spectra, *Atmos. Chem. Phys.*, 7, 1503– 1522, doi:10.5194/acp-7-1503-2007, 2007.

485 Lee, B. P., Li, Y. J., Yu, J. Z., Louie, P. K. K., and Chan, C. K.: Characteristics of submicron particulate  
486 matter at the urban roadside in downtown Hong Kong – Overview of 4 months of continuous high-  
487 resolution aerosol mass spectrom- eter measurements, *J. Geophys. Res.-Atmos.*, 120, 7040–7058,  
488 <https://doi.org/10.1002/2015JD023311>, 2015.

489 Li, H., Zhang, Q., Zhang, Q., Chen, C., Wang, L., Wei, Z., Zhou, S., Parworth, C., Zheng, B., Canonaco,  
490 F., Prévôt, A. S. H., Chen, P., Zhang, H., Wallington, T. J., and He, K.: Wintertime aerosol  
491 chemistry and haze evolution in an extremely polluted city of the North China Plain: significant  
492 contribution from coal and biomass combustion, *Atmos. Chem. Phys.*, 17, 4751–4768,  
493 <https://doi.org/10.5194/acp-17-4751-2017>, 2017.

494 Li, Y. J., Lee, B. P., Su, L., Fung, J. C. H., and Chan, C. K.: Seasonal characteristics of fine particulate  
495 matter (PM) based on high-resolution time-of-flight aerosol mass spectrometric (HR-ToF-AMS)  
496 measurements at the HKUST Supersite in Hong Kong, *Atmos. Chem. Phys.*, 15, 37-53,  
497 <https://doi.org/10.5194/acp-15-37-2015>, 2015.

498 Lim, Y. B., Tan, Y., and Turpin, B. J.: Chemical insights, explicit chemistry, and yields of secondary  
499 organic aerosol from OH radical oxidation of methylglyoxal and glyoxal in the aqueous phase,  
500 *Atmos. Chem. Phys.*, 13, 8651–8667, <https://doi.org/10.5194/acp-13-8651-2013>, 2013.

501 Liu, Y., Siekmann, F., Renard, P., El Zein, A., Salque, G., El Haddad, I., Temime-Roussel, B., Voisin,  
502 D., Thissen, R., Monod, A., 2012. Oligomer and SOA formation through aqueous phase  
503 photooxidation of methacrolein and methyl vinyl ketone. *Atmos. Environ.* 49, 123-129.

504 Mohr, C., DeCarlo, P. F., Heringa, M. F., Chirico, R., Slowik, J. G., Richter, R., Reche, C., Alastuey, A.,  
505 Querol, X., Seco, R., Peñuelas, J., Jiménez, J. L., Crippa, M., Zimmermann, R., Baltensperger, U.,  
506 and Prévôt, A. S. H.: Identification and quantification of organic aerosol from cooking and other  
507 sources in Barcelona using aerosol mass spectrometer data, *Atmos. Chem. Phys.*, 12, 1649–1665,  
508 <https://doi.org/10.5194/acp-12-1649-2012>, 2012.

509 Molteni, U., Bianchi, F., Klein, F., El Haddad, I., Frege, C., Rossi, M.J., Dommen, J., Baltensperger, U.,  
510 2018. Formation of highly oxygenated organic molecules from aromatic compounds. *Atmos.*  
511 *Chem. Phys.* 18, 1909-1921.

512 Ng, N. L., Canagaratna, M. R., Zhang, Q., Jimenez, J. L., Tian, J., Ulbrich, I. M., Kroll, J. H., Docherty,  
513 K. S., Chhabra, P. S., Bahreini, R., Murphy, S. M., Seinfeld, J. H., Hildebrandt, L., Donahue, N.  
514 M., DeCarlo, P. F., Lanz, V. A., Prévôt, A. S. H., Dinar, E., Rudich, Y., and Worsnop, D. R.:  
515 Organic aerosol components observed in Northern Hemispheric datasets from Aerosol Mass  
516 Spectrometry, *Atmos. Chem. Phys.*, 10, 4625–4641, <https://doi.org/10.5194/acp-10-4625-2010>,  
517 2010.

518 Ng, N. L., Canagaratna, M. R., Jimenez, J. L., Chhabra, P. S., Seinfeld, J. H., and Worsnop, D. R.:  
519 Changes in organic aerosol composition with aging inferred from aerosol mass spectra, *Atmos.  
520 Chem. Phys.*, 11, 6465–6474, <https://doi.org/10.5194/acp-11-6465-2011>, 2011.

521 Qin, Y. M., Tan, H. B., Li, Y. J., Schurman, M. I., Li, F., Canonaco, F., Prévôt, A. S. H., and Chan, C.  
522 K.: Impacts of traffic emissions on atmospheric particulate nitrate and organics at a downwind site  
523 on the periphery of Guangzhou, China, *Atmos. Chem. Phys.*, 17, 10245–10258,  
524 <https://doi.org/10.5194/acp-17-10245-2017>, 2017.

525 Rivellini, L.-H., Adam, M. G., Kasthuriarachchi, N., and Lee, A. K. Y.: Characterization of carbonaceous  
526 aerosols in Singapore: insight from black carbon fragments and trace metal ions detected by a soot  
527 particle aerosol mass spectrometer, *Atmos. Chem. Phys.*, 20, 5977–5993,  
528 <https://doi.org/10.5194/acp-20-5977-2020>, 2020.

529 Schöne, L. and Herrmann, H.: Kinetic measurements of the reactivity of hydrogen peroxide and ozone  
530 towards small atmospherically relevant aldehydes, ketones and organic acids in aqueous solutions,  
531 *Atmos. Chem. Phys.*, 14, 4503–4514, <https://doi.org/10.5194/acp-14-4503-2014>, 2014.

532 Sun, Y. L., Zhang, Q., Anastasio, C., and Sun, J.: Insights into secondary organic aerosol formed via  
533 aqueous-phase reactions of phenolic compounds based on high resolution mass spectrometry,  
534 *Atmos. Chem. Phys.*, 10, 4809–4822, <https://doi.org/10.5194/acp-10-4809-2010>, 2010.

535 Sun, Y. L., Wang, Z. F., Fu, P. Q., Yang, T., Jiang, Q., Dong, H. B., Li, J., and Jia, J. J.: Aerosol  
536 composition, sources and processes during wintertime in Beijing, China, *Atmos. Chem. Phys.*, 13,  
537 4577–4592, <https://doi.org/10.5194/acp-13-4577-2013>, 2013.

538 Sun, Y. L., Wang, Z. F., Du, W., Zhang, Q., Wang, Q. Q., Fu, P. Q., Pan, X. L., Li, J., Jayne, J., and  
539 Worsnop, D. R.: Long-term real-time measurements of aerosol particle composition in Beijing,  
540 China: seasonal variations, meteorological effects, and source analysis, *Atmos. Chem. Phys.*, 15,  
541 10149–10165, <https://doi.org/10.5194/acp-15-10149-2015>, 2015.

542 Sun, Y., Du, W., Fu, P., Wang, Q., Li, J., Ge, X., Zhang, Q., Zhu, C., Ren, L., Xu, W., Zhao, J., Han, T.,  
543 Worsnop, D. R., and Wang, Z.: Primary and secondary aerosols in Beijing in winter: sources,  
544 variations and processes, *Atmos. Chem. Phys.*, 16, 8309–8329, <https://doi.org/10.5194/acp-16-8309-2016>, 2016.

546 Sun, Y., Xu, W., Zhang, Q., Jiang, Q., Canonaco, F., Prévôt, A.S.H., Fu, P., Li, J., Jayne, J., Worsnop,  
547 D.R., Wang, Z., 2018. Source apportionment of organic aerosol from 2-year highly time-resolved  
548 measurements by an aerosol chemical speciation monitor in Beijing, China. *Atmos. Chem. Phys.*  
549 18, 8469–8489. <https://doi.org/10.5194/acp-18-8469-2018>

550 Wang, L. T., Wei, Z., Yang, J., Zhang, Y., Zhang, F. F., Su, J., Meng, C. C., and Zhang, Q.: The 2013  
551 severe haze over southern Hebei, China: model evaluation, source apportionment, and policy  
552 implications, *Atmos. Chem. Phys.*, 14, 3151–3173, doi:10.5194/acp-14-3151-2014, 2014.

553 Wang J, Ye J, Zhang Q, et al. Aqueous production of secondary organic aerosol from fossil-fuel  
554 emissions in winter Beijing haze. *Proceedings of the National Academy of Sciences*, 118(8):  
555 e2022179118, <https://doi.org/10.1073/pnas.2022179118>, 2021.

556 Waxman, E.M., Dzepina, K., Ervens, B., Lee-Taylor, J., Aumont, B., Jimenez, J.L., Madronich, S.,  
557 Volkamer, R., 2013. Secondary organic aerosol formation from semi- and intermediate-volatility  
558 organic compounds and glyoxal: relevance of O/C as a tracer for aqueous multiphase chemistry.  
559 *Geophys. Res. Lett.* 40, 978-982.

560 Xu, S., Liu, W., Tao, and S. Emission of Polycyclic Aromatic Hydrocarbons in China. *Biophys. Process.*  
561 *Anthropog. Org. Compd. Environ. Syst.* 40, 267–281.  
562 <https://doi.org/10.1002/9780470944479.ch11>, 2006.

563 Xu, J., Shi, J., Zhang, Q., Ge, X., Canonaco, F., Prévôt, A. S. H., Vonwiller, M., Szidat, S., Ge, J., Ma,  
564 J., An, Y., Kang, S., and Qin, D.: Wintertime organic and inorganic aerosols in Lanzhou, China:  
565 sources, processes, and comparison with the results during summer, *Atmos. Chem. Phys.*, 16,  
566 14937–14957, <https://doi.org/10.5194/acp-16-14937-2016>, 2016.

567 Xu W, Han T, Du W, et al. Effects of aqueous-phase and photochemical processing on secondary organic  
568 aerosol formation and evolution in Beijing, China. *Environmental Science & Technology*, 51(2):  
569 762-770, <https://doi.org/10.1021/acs.est.6b04498>, 2017.

570 Xu, W., Sun, Y., Wang, Q., Zhao, J., Wang, J., Ge, X., Xie, C., Zhou, W., Du, W., Li, J., Fu, P., Wang,  
571 Z., Worsnop, D. R., Coe, H., Changes in aerosol chemistry from 2014 to 2016 in winter in Beijing:  
572 Insights from high-resolution aerosol mass spectrometry. *J. Geophys. Res.-Atmos.* 124, 1132-1147,  
573 2019a.

574 Xu, W., Xie, C., Karnezi, E., Zhang, Q., Wang, J., Pandis, S. N., Ge, X., Zhang, J., An, J., Wang, Q.,  
575 Zhao, J., Du, W., Qiu, Y., Zhou, W., He, Y., Li, Y., Li, J., Fu, P., Wang, Z., Worsnop, D. R., and  
576 Sun, Y.: Summertime aerosol volatility measurements in Beijing, China, *Atmos. Chem. Phys.*, 19,  
577 10205–10216, <https://doi.org/10.5194/acp-19-10205-2019>, 2019b.

578 Zhang, Q., Jimenez, J. L., Canagaratna, M. R., et al.: Ubiquity and dominance of oxygenated species in  
579 organic aerosols in anthropogenically-influenced Northern Hemisphere midlatitudes, *Geophys.*  
580 *Res. Lett.*, 34, L13801, doi:10.1029/2007GL029979, 2007.

581 Zhang, J. K., Sun, Y., Liu, Z. R., Ji, D. S., Hu, B., Liu, Q., and Wang, Y. S.: Characterization of  
582 submicron aerosols during a month of serious pollution in Beijing, 2013, *Atmos. Chem. Phys.*, 14,  
583 2887–2903, <https://doi.org/10.5194/acp-14-2887-2014>, 2014.

584 Zhang, X., Xu, J., Kang, S., Zhang, Q., and Sun, J.: Chemical characterization and sources of submicron  
585 aerosols in the northeastern Qinghai-Tibet Plateau: insights from high-resolution mass  
586 spectrometry, *Atmos. Chem. Phys.*, 19, 7897–7911, <https://doi.org/10.5194/acp-19-7897-2019>,  
587 2019.

588 Zhang, Z., Zhu, W., Hu, M., Liu, K., Wang, H., Tang, R., Shen, R., Yu, Y., Tan, R., Song, K., Li, Y.,  
589 Zhang, W., Zhang, Z., Xu, H., Shuai, S., Li, S., Chen, Y., Li, J., Wang, Y., and Guo, S.: Formation  
590 and evolution of secondary organic aerosols derived from urban-lifestyle sources: vehicle exhaust  
591 and cooking emissions, *Atmos. Chem. Phys.*, 21, 15221–15237, [https://doi.org/10.5194/acp-21-  
592 15221-2021](https://doi.org/10.5194/acp-21-15221-2021), 2021.

593 Zhao L , Wang L , Tan J , et al. Changes of chemical composition and source apportionment of PM2.5  
594 during 2013-2017 in urban Handan, China. *Atmospheric Environment*, 206(JUN.):119-131, 2019

595 Zhou, S., Collier, S., Jaffe, D. A., Briggs, N. L., Hee, J., Sedlacek III, A. J., Kleinman, L., Onasch, T. B.,  
596 and Zhang, Q.: Regional influence of wildfires on aerosol chemistry in the western US and insights  
597 into atmospheric aging of biomass burning organic aerosol, *Atmos. Chem. Phys.*, 17, 2477–2493,  
598 <https://doi.org/10.5194/acp-17-2477-2017>, 2017.